

HST Proper Motion confirms the optical identification of the nearby pulsar PSR 1929+10¹

Roberto P. Mignani

European Southern Observatory, Karl Schwarzschild Str. 2, D-85740, Garching, Germany

rmignani@eso.org

Andrea De Luca, Patrizia A. Caraveo

*Istituto di Astrofisica Spaziale e Fisica Cosmica, Sezione di Milano "G. Occhialini" - CNR
v. Bassini 15, I-20133 Milan, Italy*

deluca@mi.iasf.cnr.it, pat@mi.iasf.cnr.it

Werner Becker

Max Planck Institute für Extraterrestrische Physik, D-85748, Garching, Germany

web@mpe.mpg.de

ABSTRACT

We report on the proper motion measurement of the proposed optical counterpart of the X-ray/radio pulsar PSR 1929+10. Using images obtained with the HST/STIS (average epoch 2001.73) we computed a yearly displacement of $+97 \pm 1$ mas yr⁻¹ in RA and $+46 \pm 1$ mas yr⁻¹ in Dec since the epoch (1994.52) of the original HST/FOC detection. Both the magnitude and direction of the optical proper motion components are found to be fully consistent with the most recent VLBA radio measurements. This result provides an unambiguous confirmation of the pulsar optical identification. In addition, we have used the combined STIS/FOC datasets to derive information on the pulsar spectrum, which seems characterized by a power law component, apparently unrelated to the X-ray emission.

Subject headings: Optical — pulsars: individual (PSR 1929+10)

¹Based on observations with the NASA/ESA Hubble Space Telescope, obtained at the Space Telescope Science Institute, which is operated by AURA, Inc. under contract No NAS 5-26555

1. Introduction

PSR1929+10 is an old ($\sim 3 \cdot 10^6$ yrs) radio pulsar. With a distance of ~ 330 pc, determined from VLBA radio parallax measurements (Briskin et al. 2002), it is also one of the closest to the solar system. After the original X-ray detection with Einstein (Helfand 1983), pulsations at the radio period (227 ms) were discovered by ROSAT (Yancopulous et al. 1994) and later confirmed in ASCA data (Wang and Halpern 1997). The X-rays pulse profile exhibits a single, broad, peak markedly different from the sharp radio one. The X-ray spectrum can be described either by a blackbody ($T \sim 3 - 5 \cdot 10^6$ K) produced from hot polar caps (Yancopulous et al. 1994; Wang and Halpern 1997) or by a power law with $\alpha \approx 1.27 \pm 0.4$ (Becker and Trümper 1997). A trail of diffuse X-ray emission originated from the pulsar and extending ~ 10 arcmin to South East was discovered with the ROSAT/PSPC (Wang et al. 1993). A candidate optical counterpart to PSR1929+10 was identified with the HST/FOC by Pavlov et al. (1996) based on the positional coincidence ($\sim 0''.4$) with the radio coordinates. Interestingly, the measured flux of the PSR1929+10 counterpart ($U \sim 25.7$) was found to deviate by 3 orders of magnitude from the values predicted from the X-ray spectra. This behaviour is markedly different from that of the middle aged pulsars PSR0656+14 (Pavlov et al. 1997), Geminga (Mignani et al. 1998) and PSR1055-52 (Mignani et al. 1997), where the optical data are not too far from the extrapolation of the X ray spectra. Confirming the optical identification of PSR1929+10 becomes a crucial step to settle a consistent scenario for the long term evolution of the optical luminosity of pulsars and to investigate possible turnovers in the emission physics. While young ($\sim 10^3 - 10^4$ yrs) objects are relatively bright, their optical throughput seems to decay on a timescale of few thousands years and progressively turn to a composite magnetospheric/thermal regime (Mignani 1998; Caraveo 2000). Although evidence for such a trend can be recognized in middle-aged objects ($\sim 10^5$ yrs), like PSR 0656+14 and Geminga, little is known on the optical emission at later stages of the pulsar lifetime.

Taking advantage of new HST observations, we use the pulsar proper motion to secure the PSR 1929+10 optical identification, thus adding an important piece of information on the optical behaviour of old pulsars. Observations and data reduction are described in §2, while the results are discussed in §3.

2. Observations

The field of PSR 1929+10 was observed with the STIS detector aboard HST in five different visits on August 28th 2001, September 11th, 15th, 21st 2001, October 20th 2001. The observations were performed after the reactivation of the STIS following problems with

the power supply units occurred in May 2001. Owing to this malfunction, the observations could have been affected by a residual few percent increase of the dark current level. For each visit, the total integration time was 2400 s, split in two exposures of 1200 s each. Observations run smoothly apart from short gaps (~ 60 s) in the engineering telemetry occurred during visits #3 and #4. The NUV-MAMA detector, with a pixel size of $0''.024$ ($24''.7 \times 24''.7$ field of view), was used in its TIME-TAG mode to obtain time-resolved images with a temporal resolution of $125\mu\text{s}$. To add spectral information in the NUV and to complement previous data obtained with the FOC at $\sim 3400\text{\AA}$ by Pavlov et al. (1996), the exposures were taken through the F25Q7Z filter ($\lambda = 2364\text{\AA}$, $\Delta\lambda \sim 842\text{\AA}$ *FWHM*).

Our identification strategy was based on two independent and complementary approaches. Firstly, following the straightforward, but powerful, strategy successfully applied in the case of the identification of PSR 0656+14 (Mignani, De Luca and Caraveo 2000), we performed a proper motion measurement of the proposed counterpart to be compared with the known one of the radio pulsar, recently reassessed by Brisken et al. (2002) using the VLBA. Secondly, we used our time-resolved images to search for pulsations at the radio period from the candidate counterpart. The proper motion measurement is described in the following sections, while the results of the timing analysis are presented in a companion paper (Mignani et al. in preparation).

2.1. Data Analysis

As starting point for our proper motion measurement we used the FOC observations of Pavlov et al. (1996), collected on July 10th 1994. Images were taken in three different filters: F130LP ($\lambda = 3437.7\text{\AA}$, $\Delta\lambda \sim 1965\text{\AA}$ *FWHM*), F342W ($\lambda = 3402\text{\AA}$, $\Delta\lambda \sim 442\text{\AA}$ *FWHM*) and F430W ($\lambda = 3940\text{\AA}$, $\Delta\lambda \sim 832\text{\AA}$ *FWHM*), with total integration times of 1221, 3310 and 596 s, respectively. The camera was operated at two different focal lengths corresponding to a field of view of $7''.4 \times 7''.4$ for the F130LP and F342W exposures and of $14''.8 \times 14''.8$ for the F430W one. In both cases, the angular resolution was $0''.014$ per pixel. The data were retrieved from the ST-ECF public archive after on-the-fly recalibration with the best reference files. As shown by Pavlov et al. (1996), the pulsar counterpart is detected only through the F130LP and the F342W filters (see their figures 2c and 3a).

The STIS images were retrieved from the STScI data archive after the default pipeline calibration. Each image has been corrected for the geometric distortion of the CCD using the DRIZZLE software distributed in the STSDAS package² and applying the most recent coefficients of the cubic mapping of the NUV-MAMA field of view listed in the STIS Users'

²stdas.stsci.edu/STSDAS.html

Handbook³. The two exposures taken during each visit were coadded after accounting for thiny shifts (of order 0.4 pixels) and differences in roll angle (of order 0.03°) due to the spacecraft jitter. For each couple, the average coadditon accuracy was of ~ 0.1 pixels in both x and y .

Since the expected overall displacement of the pulsar counterpart (~ 15 mas, equivalent to 0.6 STIS pixels) in the epoch interval spanned by our observations (2001.65-2001.80) would be negligible with respect to the total displacement (~ 770 mas) predicted since the reference epoch (1994.52), we first combined all the five available STIS images to benefit of the higher S/N . Using as relative reference grid the coordinates of 7 to 10 common stars (the actual number depending on the telescope roll angle), all the frames were registered on the mid-epoch frame (i.e. the september 15th one) by fitting a linear coordinate transformation after aligning each frame in right ascension and declination according to the telescope roll angles. The final STIS image resulting from the combination of all the available frames is shown in Figure 1. As expected in the case of a moving object, the centering accuracy of the target in the combined image (0.3 pixels in RA and 0.15 pixels in Dec) appears degraded wrt to the values measured in each single single frame, for which we found accuracies of ~ 0.1 pixels in both coordinates. To the error on the centroid determination we then added in quadrature the rms on the epoch-to-epoch coordinate transformation, which in all cases turned out to be within 0.2 pixels (per coordinate), plus the accuracy of the exposures coaddition in each visit (0.1 pixels). The final precision on the target position in the combined STIS image was thus 0.37 pixels in RA and 0.27 pixels in Dec.

Next step was to apply the STIS-to-FOC registration to evaluate the relative displacement of the pulsar counterpart over the ~ 7.2 years interval spanned by the available observations. Although our target was clearly detected in the FOC/F130LP image (preferred to the F342W one because of its higher S/N), its $7''.4 \times 7''.4$ field of view contains only one object in common with the wider STIS image ($24''.7 \times 24''.7$). Thus, we decided to register both images on a common reference frame defined by the FOC/F430W image ($14''.8 \times 14''.8$). This allowed us to use three bright reference objects for the FOC/130LP-to-FOC/430W superposition (accounting for shift and rotation for a resulting accuracy of 0.3 FOC pixels per coordinate) and 4 good reference objects for the STIS-to-FOC/430W superposition (rms of 0.55 FOC pixels per coordinate - accounting for shift, rotation and scale factor). The overall accuracy in the final STIS-to-FOC/F130LP superposition was thus obtained by adding in quadrature all the uncertainties quoted above and turned out to be ~ 0.6 FOC pixels per coordinate.

³www.stsci.edu/hst/stis/documents/handbooks/cycle11/stis_cy11_lhbTOC.html

3. Results

3.1. Proper Motion

After registering both the FOC and the STIS images on a unique reference frame, we could evaluate the displacement of the pulsar candidate counterpart by simply measuring the difference in its relative coordinates. The overall uncertainty on such difference was estimated by adding in quadrature all the uncertainties derived from the different steps of our relative astrometry procedure. These include: the centering error of the counterpart in the combined five-epochs STIS image (0.37 STIS pixels in RA and 0.27 pixels in Dec) and in the FOC/130LP image (~ 0.1 FOC pixels per coordinate) plus the overall accuracy of the STIS-to-FOC/130LP superposition (0.6 FOC pixels per coordinate) as obtained by the two-step procedure described in the previous section. The difference in the relative coordinates is 48.7 ± 1.0 FOC pixels and 23.2 ± 1.0 FOC pixels along the RA and Dec directions, respectively. Such measurements represent a clear evidence for the object displacement over the ~ 7.2 years time span between the FOC (1994.52) and the average STIS epoch (2001.731). The pulsar displacement can be appreciated in Figure 2, where the relative FOC position is overlaid on the STIS image. After applying the FOC plate scale of $0''.01435/\text{pixel}$ (with 0.5% uncertainty) to translate from pixel to sky coordinates, we computed the proper motion of the pulsar optical counterpart. This is $\mu_\alpha \cos(\delta) = +97 \pm 2 \text{ mas yr}^{-1}$ and $\mu_\delta = +46 \pm 2 \text{ mas yr}^{-1}$, corresponding to a total yearly displacement in the plane of the sky of $\mu = 107.3 \pm 1 \text{ mas yr}^{-1}$ along a position angle (PA) of $64.6^\circ \pm 0.5^\circ$. Although the FOC and STIS observations were taken at different times of the year, we did not apply any correction for the object’s parallax (Briskin et al. 2002) as the effect of the tiny parallactic displacement is well within our error budget.

As a further check, we have recomputed the pulsar displacement using the FOC/130LP image and, in turn, each of the five single-epoch STIS images. This allowed us to obtain five independent measures for five different epoch pairs (see Table 1) and thus to exclude the effects of unknown systematics in our procedure. In this case, for each STIS image the error on the target position was only due to the combination of the centering error (~ 0.1 pixels per coordinates) and the accuracy of the coaddition of the single exposures in each visit (0.1 pixels). The final precision on the target position in each of the five single-epoch STIS images was thus of the order of 0.15 pixels per coordinate. The strategy for the STIS-to-FOC/130LP registration was clearly the same described above. We computed the STIS-to-FOC/430W frame registrations (rms of 0.45 -0.65 FOC pixels per coordinate - accounting for shift, rotation and scale factor) with the same number of objects used in §2.1. The overall accuracy of the final STIS-to-FOC/130LP registrations turned out to be between 0.55 and 0.8 FOC pixels. As described above, the uncertainty on the target displacement is

due to the combination of the centering error of the counterpart in the single STIS images (0.15 original STIS pixels in both RA and Dec) and in the FOC/130LP image (0.1 FOC pixels per coordinate) plus the overall STIS-to-FOC/130LP superposition accuracy (0.55-0.8 FOC pixels per coordinate).

The proper motions derived from the displacements computed for each of the five epoch pairs are listed in Table 1, where all the values are seen to be consistent with the proper motion obtained using the combined STIS image. A χ^2 fit to the values listed in Table 1 yields the best proper motion values: $\mu_\alpha \cos(\delta) = +97 \pm 1$ mas yr⁻¹ and $\mu_\delta = +46 \pm 1$ mas yr⁻¹, corresponding to a yearly displacement $\mu = 107.35 \pm 1$ mas yr⁻¹ along a position angle of $64.63^\circ \pm 0.55^\circ$.

We can now compare our best proper motion value with the most recent radio measure obtained by Brisken et al. (2002), who give $\mu_\alpha \cos(\delta) = +94.82 \pm 0.26$ mas yr⁻¹ and $\mu_\delta = +43.04 \pm 0.15$ mas yr⁻¹ ($65.58^\circ \pm 0.09^\circ$ PA). Although our value is somewhat less precise, we note that the optical proper motion is fully consistent with the radio one. Thus, our proper motion measurement provides a robust proof that the candidate proposed by Pavlov et al. (1996) is indeed the optical counterpart of PSR 1929+10.

3.2. Photometry

We have used our STIS images to measure the pulsar flux in the F25QTZ filter. In order to take advantage of the higher S/N , our photometry has been computed on the combined image (Figure 1). The source counts were extracted using an optimized aperture and the flux conversion was applied using the photometric zeropoint provided by the pipeline STIS flux calibration. We thus derived a flux of $(5.4 \pm 0.4) \cdot 10^{-31}$ erg cm⁻² s⁻¹ Hz⁻¹, corresponding to an ST-mag of 25.4 ± 0.15 . The attached error takes into account both the accuracy of our aperture photometry and the systematic uncertainty of $\sim 5\%$ which affects the absolute flux calibration of the STIS/MAMA⁴. The measured flux was then compared with the values obtained with the FOC in the 130LP and 342W filters. For consistency, we have independently reanalyzed the FOC datasets finding flux values virtually identical to the ones reported in Pavlov et al. (1996). This confirms that the optical points are definitely inconsistent with the extrapolations of the X-ray spectra which, depending on the assumed model (power law or polar caps), predict fluxes ~ 3 orders of magnitude higher and lower, respectively. The comparison between the FOC and the STIS photometry is shown in Figure 3, where in the upper panel we plotted the measured values and in the lower panel we corrected for a likely upper limit on the extinction of $E(B - V) = 0.1$ (see Pavlov et al.

⁴www.stsci.edu/hst/stis/documents/handbooks/cycle11/stis_cy11_ihbTOC.html

1996). While the data can not be accounted by a single blackbody function, a power law provides a more straightforward fit. For the two extreme values of the extinction the power law spectral index α varies between 1 and 0, respectively. Although the data could also be compatible with a composite model, any realistic spectral fit is hampered both by the few points available and by the limited spectral coverage.

4. Conclusions

Using images collected with the STIS camera aboard HST together with archived HST/FOC images taken 7.2 years apart we have measured a very significant angular displacement of the proposed optical counterpart of PSR 1929+10. This yields a proper motion $\mu_\alpha \cos(\delta) = +97 \pm 1 \text{ mas yr}^{-1}$ and $\mu_\delta = +46 \pm 1 \text{ mas yr}^{-1}$. These values agree with the ones derived from very recent VLBA radio measurements (Briskin et al. 2002), thus providing an unambiguous confirmation of the pulsar identification. Securing the identification of an old pulsar such as PSR 1929+10 is an important step to assess the pulsars' optical behaviour as a function of their age. At variance with the phenomenology of middle aged objects, such as PSR 0656+14, Geminga and PSR 1055-52, the optical emission of PSR 1929+10 seems unrelated to the X-ray one, be it either of thermal or non-thermal origin. Although the new STIS data seem to favour a power law rather than a blackbody, the paucity of flux values and the limited spectral coverage available do not allow us to put firmer constraints on the spectrum. More data, especially at longer wavelengths, are required to better characterize the pulsar spectral shape and to unveil the possible presence of different spectral components. The detection of the optical timing signature will add an important piece of information to understand the optical behaviour of this old pulsar.

RM warmly thanks F. Patat for his help in the finalization of this observing program.

REFERENCES

- Becker, W. and Trümper, 1997, A&A 326, 682
- Briskin, W.F., Benson, J.M., Goss, W.M. and Thorsett, S.E., 2002, ApJ 571, 906
- Caraveo, P.A., 2000, in Pulsar Astronomy - 2000 and Beyond, ASP Conference Series, Vol. 202, p. 202, Eds. M. Kramer, N. Wex, and N. Wielebinski

- Helfand, D.J., 1983, in IAU Symp. 101, Supernova Remnants and Their X-ray Emissions, Eds. J. Danziger and P. Gorenstein (Dordrecht: Reidel), 471
- Mignani, R., Caraveo, P.A. and Bignami, G.F. 1997, ApJ, 474, L51
- Mignani, R., 1998, Neutron Stars and Pulsars : Thirty Years after the Discovery, Frontiers science series n. 24, p.335, Eds. N. Shibazaki et al.
- Mignani, R., Caraveo, P.A. and Bignami, G.F. 1998, A&A 332, L37
- Mignani, R.P., De Luca, A., Caraveo, P.A., 2000, ApJ 543, 318
- Pavlov, G.G., Stringfellow, G.S. and Córdova, F.A., 1996, ApJ 467, 370
- Pavlov, G.G., Welty, A.D. and Cordova, F.A. 1997 ApJ 489, L75
- Yancopoulos, A., Hamilton, T.T. and Helfand, D.J., 1994, ApJ 429, 832
- Wang, Q.D., Li, Z.-Y. and Begelman, M.C., 1993, Nature 364, 127
- Wang, F.Y.-H., and Halpern, J.P., 1997, ApJ 482, L159

| Pair | Epoch #1 | Epoch #2 | $\mu_{\alpha\cos(\delta)}$ | μ_{δ} | μ | PA |
|------|----------|----------|----------------------------|----------------|-----------|------------|
| 1 | 1994.52 | 2001.654 | 97.0±1.4 | 46.0±1.4 | 107.3±1.4 | 64.63±0.75 |
| 2 | 1994.52 | 2001.695 | 97.7±1.5 | 44.8±1.5 | 107.5±1.5 | 65.36±0.80 |
| 3 | 1994.52 | 2001.704 | 96.6±1.6 | 48.6±1.6 | 108.1±1.6 | 63.29±0.84 |
| 4 | 1994.52 | 2001.720 | 96.7±1.3 | 45.8±1.3 | 107.0±1.3 | 64.65±0.70 |
| 5 | 1994.52 | 2001.808 | 96.8±1.3 | 45.5±1.3 | 106.9±1.3 | 64.87±0.69 |

Table 1: Summary of the proper motion measures obtained by comparing the original pulsar position derived from the FOC observation of Pavlov et al. (1996) with those derived from each of the five available STIS observations (see text). Column 1 numbers the epoch pairs, column 2 gives the reference epoch of the FOC observation while column 3 gives the epochs of the STIS observations. The derived proper motion values (mas/yr) in RA and Dec, the total proper motion and the position angle (degrees) are listed in columns 4 to 7, respectively.

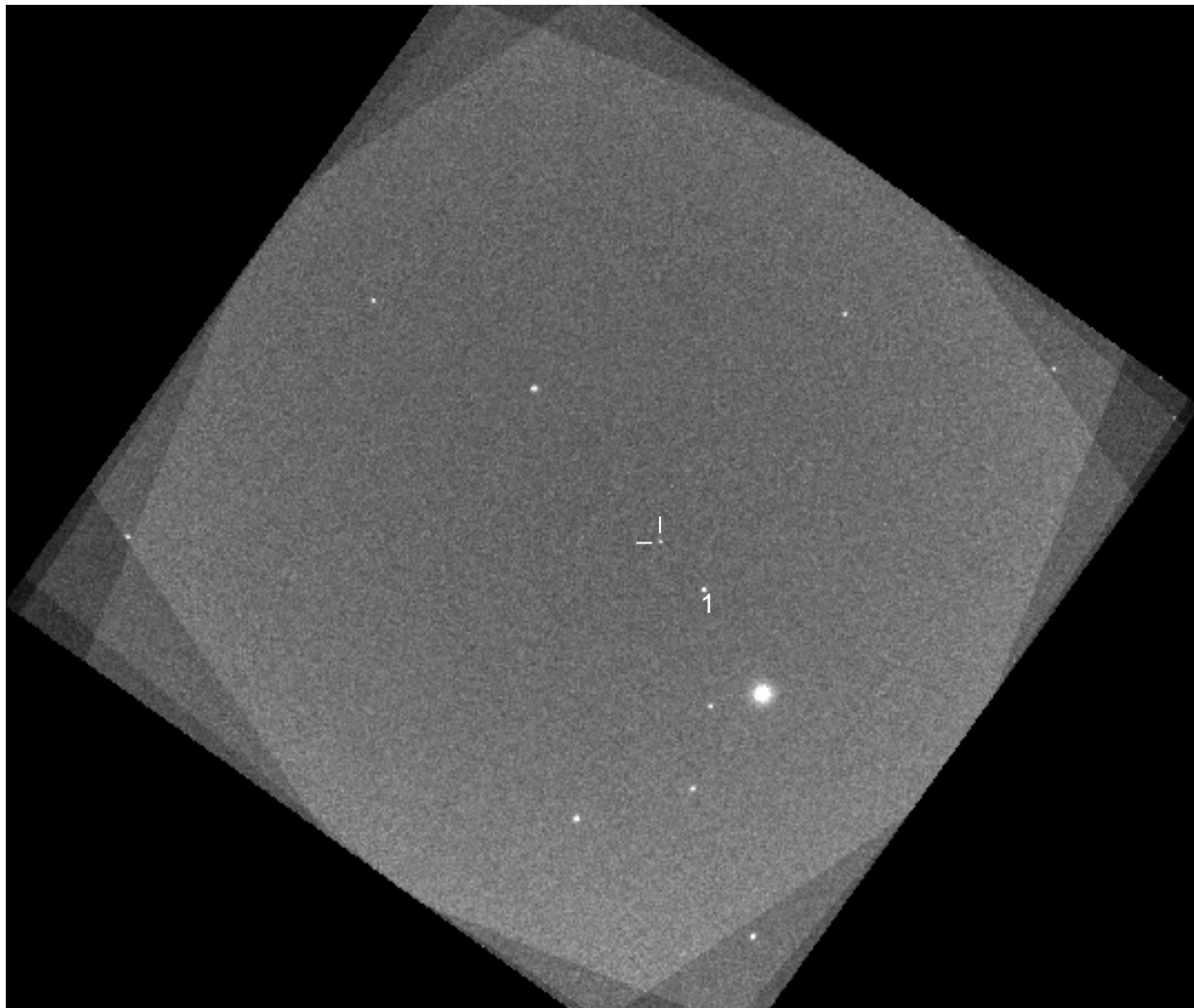


Fig. 1.— STIS/NUV-MAMA image of the field of PSR 1929+10 taken through the F25QTZ filter (epoch 2001.73). The image is the result of the combination of 10 exposures taken at five different epochs for a total exposure time of 12 000 s (see text). The frame is aligned in Right Ascension and Declination (North to the top, East to the left). The difference in the exposure map across the field is due to the coaddition of images taken with different roll angles. The pulsar candidate counterpart is marked by the two ticks. As a reference, we have labelled star 1 from Figure 2c of Pavlov et al. (1996)



Fig. 2.— Close-up of Figure 1 centered around the pulsar position. The cross marks the relative coordinates of the pulsar at epoch 1994.52, corresponding to the FOC observations of Pavlov et al. (1996). The pulsar displacement in 7.2 years is evident.

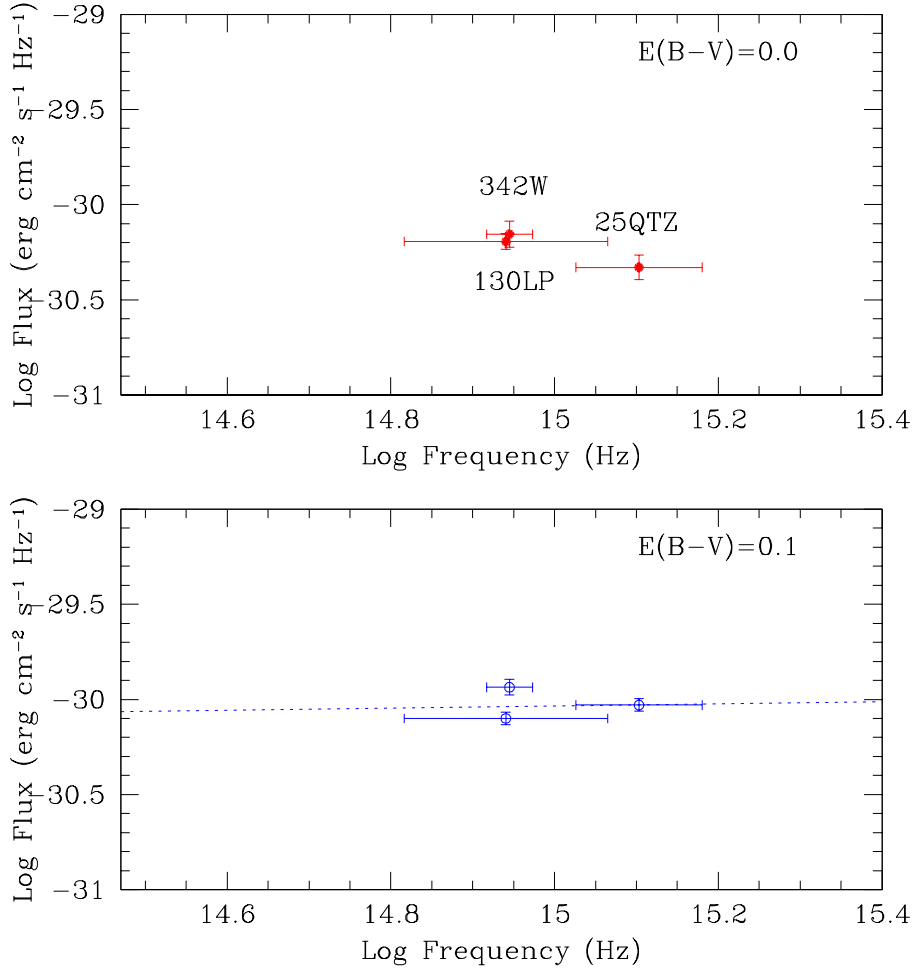


Fig. 3.— Flux of the PSR 1929+10 counterpart in the STIS 25QTZ filter compared with the FOC measurements in the 130LP and 342W passbands (Pavlov et al. 1996). In the upper panel no correction for the interstellar extinction has been applied. In the lower panel, the fluxes have been corrected for an interstellar extinction of $E(B - V) = 0.1$. In both cases, the dashed line represents the power law best fitting the spectral data.